Single-Axis Control of a Solar Sail Through a Gimbal

Johnathan Clouse*
University of Colorado, Boulder, CO, 80309-0429, USA

*Graduate Student, Aerospace Engineering Sciences, 1111 Engineering Drive, Boulder, CO, 80309-0429

Contents

I. Introduction

Single-axis control of a solar-sail-driven interplanetary spacecraft (sailcraft) is proposed. The attitude control system will be responsible for ensuring that the steering angle between the force and velocity vectors is within the tolerance necessary for an interplanetary voyage. This steering angle is dependent on the mission parameters and the orbital position of the spacecraft. The steering angle results in a commanded angle betwee the sail normal vector and the sun vector. For orbit-raising maneuvers on a sun-orbity spacecraft, the highest sun angle commanded would be 35° [McInnes]. All torques are assumed to happen about the spacecraft yaw axis, which is parallel to the orbit normal. A diagram of the system can be seen in Figure 1.

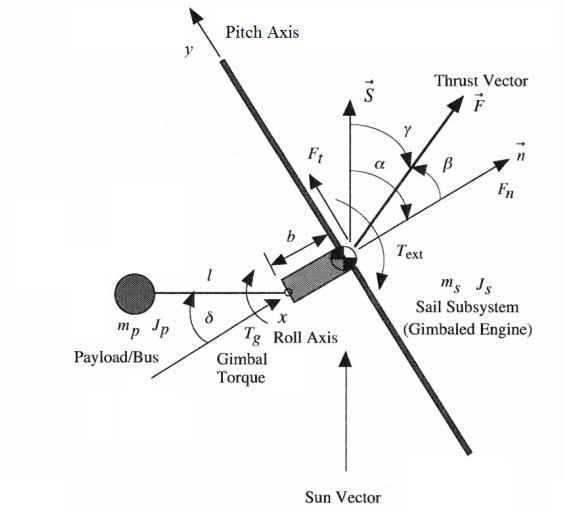

Figure 1. Diagram of the spacecraft [Wie].

The primary actuation mechanism will be a gimbaled control boom between the sail subsystem and the spacecraft bus, which contains the majority of the spacecraft mass. With the center of mass between the thrust point and the sun, expected disturbances will cause oscillation about some angle between the sun and the axis normal to the sail, α, for a locked gimbal. Changing the gimbal angle, δ, will dampen this oscilation with the right conrol law. Roll and pitch angles wil be held to zero for this analysis. Sun sensors will determine spacecraft yaw, and will have a maximum error of $\pm 0.05°$.

The state-space model has four states: the sun angle (α), the rate of the sun angle ($\dot{\alpha}$), the gimbal angle (δ), and the gimbal angle rate ($\dot{\delta}$).

The sail and boom will be modeled as rigid bodies, justified by the slow actuation of the gimbal throughout the flight. The sail will be modeled as a thin plate, rather than a billowed sail. Solar pressure torques (about the non-steered axis) will be controlled against.

The state-space model was obtained in a similar manner to that presented by Wie. The equations of motion for a gimbaled thrust vector were obtained for the yaw axis.

System performance was judged by the response to errors, namely a step from α=0° to α=35°. Mitigation of disturbance torques will also be examined.

II. System Model

The equations of motion were linearized about the state $\alpha = \dot{\alpha} = \delta = \dot{\delta} = 0$. This state is in equilibrium, due to the the force resulting from the solar radiation pressure acting through the sailcraft's center of mass.

Any disturbance to α would cause oscillation about $\alpha = 0$. The linearized equations are shown below [Wie]:

$$[J_s + (m_s m_p/m)b(b+l)]\ddot{\alpha} + (m_s m_p/m)bl\ddot{\delta} = -(m_p/m)bF_t - T_g + T_{ext} \tag{1}$$

$$[J_p + (m_s m_p/m)l(b+l)]\ddot{\alpha} + [J_p + (m_s m_p/m)l^2]\ddot{\delta} = -(m_p/m)lF_t + (m_p/m)lF_n\delta + T_g \tag{2}$$

The state-space model form is:

$$\begin{bmatrix} \dot{\alpha} \\ \ddot{\alpha} \\ \dot{\delta} \\ \ddot{\delta} \end{bmatrix} = \begin{bmatrix} 0 & 1 & 0 & 0 \\ \frac{-m_p b F_{t\ max}(\frac{J_p m}{J_p m + m_s m_p l(l-bZ)})}{J_s m + m_s m_p b(b+l)} & 0 & \frac{-m_s m_p bl \frac{-m_p l F_{n\ max}}{J_p m + m_s m_p l(l-bZ)}}{J_s m + m_s m_p b(b+l)} & 0 \\ 0 & 0 & 0 & 1 \\ \frac{m_p(-l+bZ)F_{t\ max}}{J_p m + m_s m_p l(l-bZ)} & 0 & \frac{-m_p l F_{n\ max}}{J_p m + m_s m_p l(l-bZ)} & 0 \end{bmatrix} \begin{bmatrix} \alpha \\ \dot{\alpha} \\ \delta \\ \dot{\delta} \end{bmatrix} + \begin{bmatrix} 0 \\ -\frac{1}{J_s} \\ 0 \\ \frac{1}{J_p + \frac{m_s m_p}{m} l^2} \end{bmatrix} T_{gimbal} \tag{3}$$

$$y = \begin{bmatrix} 1 & 0 & 0 & 0 \end{bmatrix} x + \begin{bmatrix} 0 \end{bmatrix} u \tag{4}$$

where

$$F_{n\ max} = PA(1 + \rho_s + \frac{2}{3}\rho_d) \tag{5}$$

$$F_{t\ max} = PA(1 - \rho_s) \tag{6}$$

$$Z = \frac{J_p + \frac{m_s m_p}{m} l(b+l)}{J_s + \frac{m_s m_p}{m} b(b+l)} \tag{7}$$

Table 1. Sailcraft characteristics [Wie].

Characteristic	Value
m_s	40 kg
m_p	116 kg
m	156 kg
J_s	6000 kg·m^2
J_p	20 kg·m^2
P	4.563e-6 kg/m^2
A_{sail}	1800 m^2
l	2 m
d	1.487 m
ρ_s	0.8272
ρ_d	-0.5949

Using the sailcraft characteristics in Table 1, the rank of A is found to be 4 and the eigenvalues are found to be:

$$\lambda_i = \{\pm j1.1244 \times 10^{-2}, \pm j2.9573 \times 10^{-4}\}.$$

The complex eigenvalues with no real parts indicate that the uncontrolled, linearized system is marginally stable. It will oscillate undamped when perturbed by a small amount, but a large disturbance could excite the modes and make the output y unbounded. However, as α and δ each approach $\pm 90°$, the assumption becomes invalid. Indeed, in Figure 2, one can see that a five-percent error between the non-linear and linearized sail force occurs at approximately $\pm 20°$.

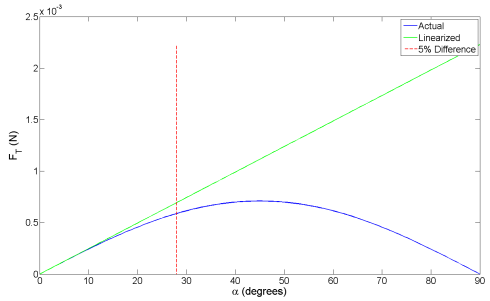

(a) Transverse force

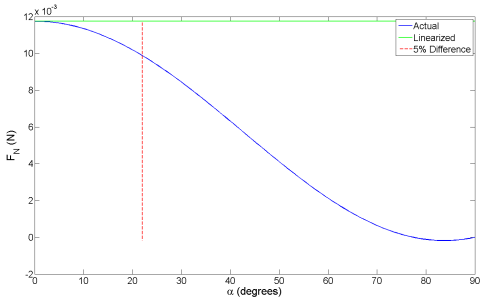

(b) Normal force

Figure 2. Linear solutions of the sail forces vs. sun angle.

The gimbal angle will be kept within $\pm 30°$ so that large responses will not mask the dynamics and keep the sun angle slow-moving. The system model will be within the realm of linearity for the highest commanded α. The controller will have to dampen the oscillations induced induced by disturbances so that the sail can provide a force in the desired direction. Overshoot will be permissible, but must not exceed 10% of the maximum commanded α. There must be zero steady-state error, since the controller would be expected to track a slowly-changing commanded α with no error.

The uncontrolled step response of the system is shown in Figure 3. The response confirms the prediction from the eigenvalues: a sine-wave response for small step inputs, and unbounded response after some threshold. Because the eigenvalues have no real part, the motion is undamped.

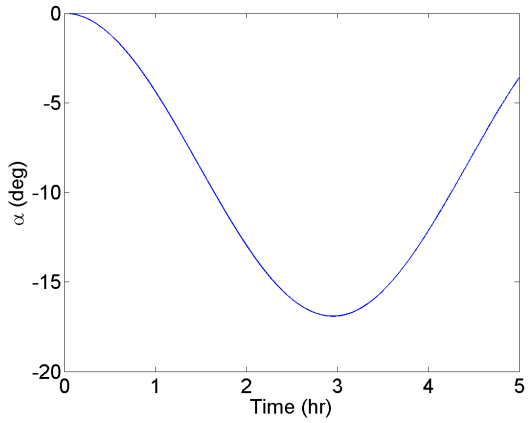

(a) Stable, $T_g = 10^{-4}$ N-m

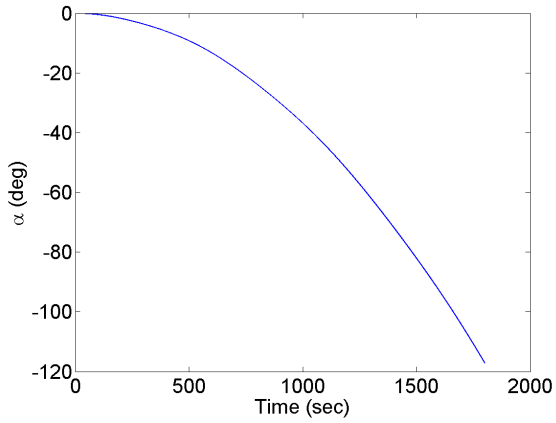

(b) Unstable, $T_g = 10^{-2}$ N-m

Figure 3. Open-loop responses.

Reachability is determined by comparing the rank of the controllability matrix with the rank of the open-loop system. The controllability matrix P turns out to be

$$P = \begin{bmatrix} B & AB & A^2B & A^3B \end{bmatrix} = \begin{bmatrix} 0 & -1.6564 \times 10^{-4} & 0 & 4.6394 \times 10^{-9} \\ -1.6564 \times 10^{-4} & 0 & 4.6394 \times 10^{-9} & 0 \\ 0 & 7.4412 \times 10^{-3} & 0 & -9.3875 \times 10^{-7} \\ 7.4412 \times 10^{-3} & 0 & -9.3875 \times 10^{-7} & 0 \end{bmatrix} \tag{8}$$

The rank of the controllability matrix is 4, as is the rank of the system matrix A. Thus, the system is controllable. Because A is full rank, controllability implies reachability, so the system is actually reachable.

Observability is determined by comparing the rank of the observability matrix with the rank of the open-loop system. The observability matrix O is

$$O = \begin{bmatrix} C \\ CA \\ CA^2 \\ CA^3 \end{bmatrix} = \begin{bmatrix} 1.0000 & 0 & 0 & 0 \\ 0 & 1.0000 & 0 & 0 \\ -1.2654 \times 10^{-8} & 0 & 6.2320 \times 10^{-7} & 0 \\ 0 & -1.2654 \times 10^{-8} & 0 & 6.2320 \times 10^{-7} \end{bmatrix} \tag{9}$$

The rank of the observability matrix is 4. Thus, the system is observable.

III. State Feedback from Manual Pole Placement

The design parameters were chosen to be as follows: for a state at the origin, control the sun angle to 35° in 90 minutes (within 5%) with no more than 10% overshoot and without violating the actuator limits defined previously. This slew is actually fairly fast compared to the nominal steering, but would be useful for attitude maneuvers needed to meet payload or communications constraints, or recovering from a fault en route. An integral term was also implemented to drive the steady-state error of the sun angle to zero while being robust to disturbances and plant errors. The poles were then chosen such that the dominant poles for a damped harmonic oscilator would have these characteristics. The other complex conjugate poles were placed to the left of the dominant poles by 0.1 on the real axis. The final pole was picked to be far to the left of the dominant poles, at -100. With the poles placed, the full-state feedback gains were:

$$\begin{aligned} K &= \begin{bmatrix} K_\alpha & K_\delta & K_{\dot{\alpha}} & K_{\dot{\delta}} & K_i \end{bmatrix} \\ &= \begin{bmatrix} -7.4967 \times 10^4 & -6.3124 \times 10^7 & 1.0524 \times 10^3 & -1.3917 \times 10^6 & 59.557 \end{bmatrix} \end{aligned} \tag{10}$$

Figure 4 shows the response of a sail starting at $\alpha = \delta = 0°$ being controlled to $\alpha = 35°$.

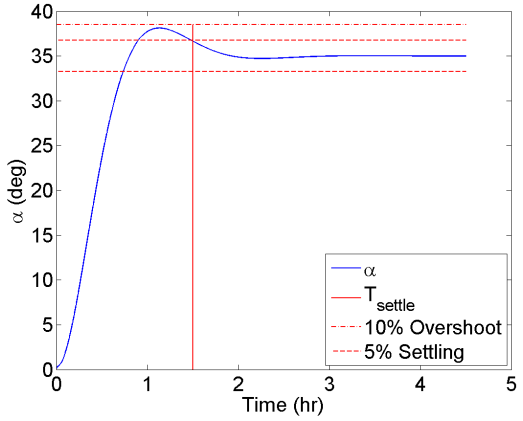

(a) α response

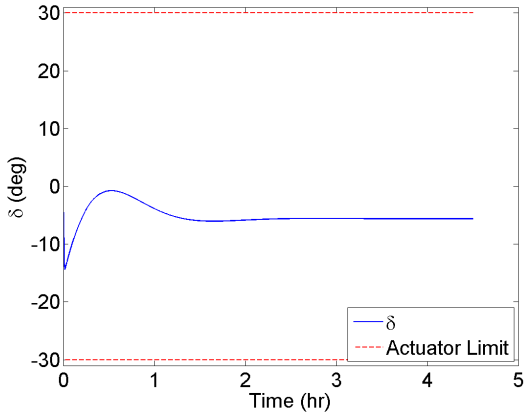

(b) δ response

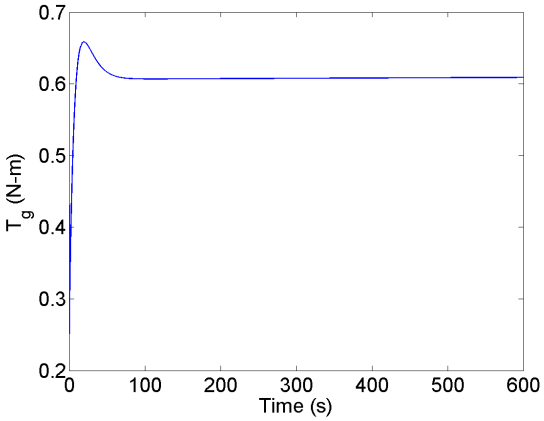

(c) Gimbal torque

Figure 4. System response of controller with manually placed poles, commanded $\alpha = 35°$.

One can see from the results that the controller met the design criteria. The underdamped motion of α is expected due to the complex-conjugate eigenvalue pairs. The gimbal tourque is a maximum of 0.35 N-m to maximize the initial change in α, and settles the value required to hold the sail/bus configuration as α settles. The gimbal angle δ settles to a non-zero trim position to keep α at its reference value. This result is practical given that the actuator limit is not violated. The gimbal torque, which is the control effort, is also less compared to that of comparable systems [Wie].

IV. Observer Design

A Luenberger observer was designed to reconstruct the state from sun-angle measurements. The Luenberger gains L were tuned by placing poles on the negative-real axis until the previously-studied step response produced a gimbal angle within the limits and the gimbal torque was minimized for an observer error at the maximum sensor inaccuracy.

$$\begin{aligned} L &= \begin{bmatrix} L_\alpha & L_\delta & L_{\dot{\alpha}} & L_{\dot{\delta}} \end{bmatrix} \\ &= \begin{bmatrix} -3.7246 \times 10^5 & -5.9012 \times 10^7 & -5.4575 \times 10^3 & -1.3001 \times 10^6 \end{bmatrix} \end{aligned} \tag{11}$$

For an initial error of zero, the observer implementation performed the same as the previously-analyzed controlled system. However, with an error in sun angle of 0.05°, the results differed. The previously-defined controller response with the observer implementation and initial error are shown in Figure 5.

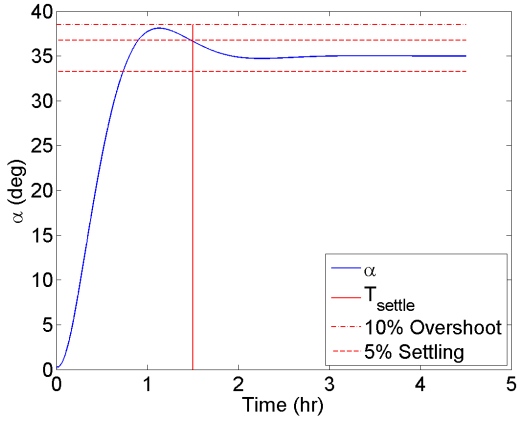

(a) α response

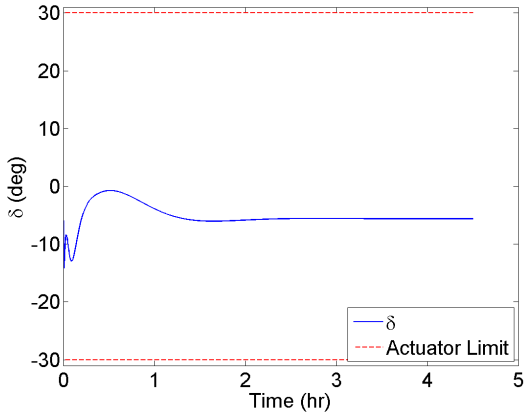

(b) δ response

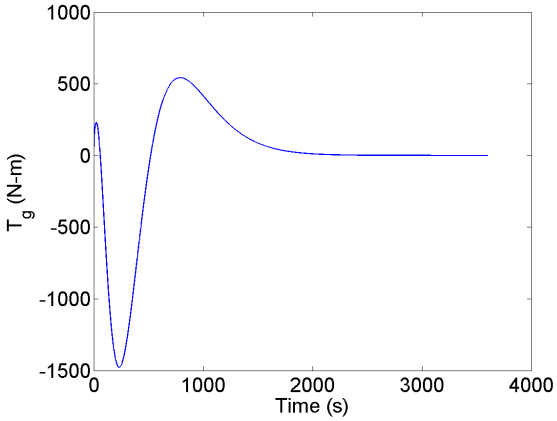

(c) Gimbal torque

Figure 5. System response of controller with observer implemented, commanded $\alpha = 35°$, 0.05° sun angle initial error.

The controller still meets the design criteria. However, the torque magnitude is drastically increased, though still feasible to implement on a spacecraft. The additional control effort, which greatly fluctuates the gimbal angle initially, is the most visible result compared to the implementation without the observer. Sensor noise could have a large effect, as the system works hard to rectify a small observer error. Further study should involve realistic sensor noise and filtering techniqes. Figure 6 shows all observer error being driven to zero.

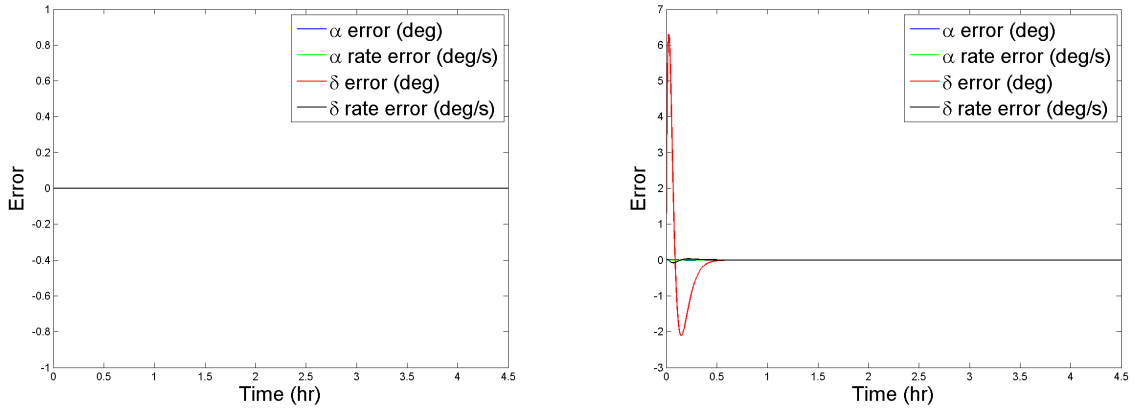

(a) No initial error

(b) 0.05° initial error in sun angle

Figure 6. Observer errors.

V. Optimal Control

A linear-quadratic regulator (LQR) controller was implemented, with the cost function

$$J = \int_0^\infty \left(x^T(t)Qx(t) + u^T(t)Ru(t)\right) dt \tag{12}$$

where Q weights the state and R weights the control effort. After tuning with Bryson's method, the weights and resulting gains were found to be

$$\begin{gathered} Q = diag(\begin{bmatrix} 4.0496 \times 10^{-9} & 9.9920 \times 10^{-5} & 3.6446 & 9.9920 \times 10^{-5} & 9.9920 \times 10^{-5} \end{bmatrix}) \\ R = 10 \\ K_{LQR} = \begin{bmatrix} -2.6947 & -1.2308 \times 10^{-3} & 5.8316 \times 10^{-1} & -1.4250 \times 10^{1} & 3.1610 \times 10^{-3} \end{bmatrix} \end{gathered} \tag{13}$$

Figure 7 shows the implementation of the LQR controller with the previously-derived observer, without initial observer error.

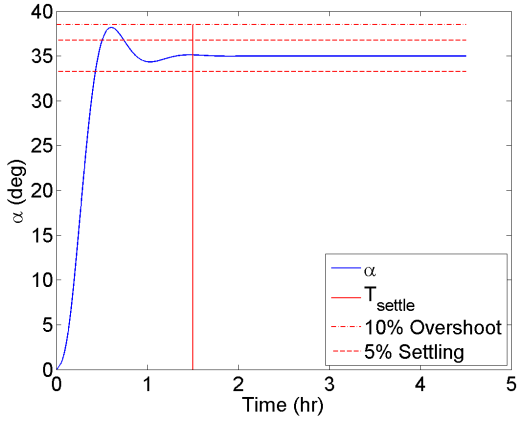

(a) α response

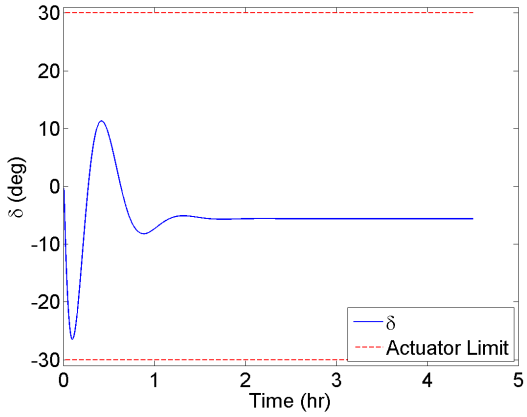

(b) δ response

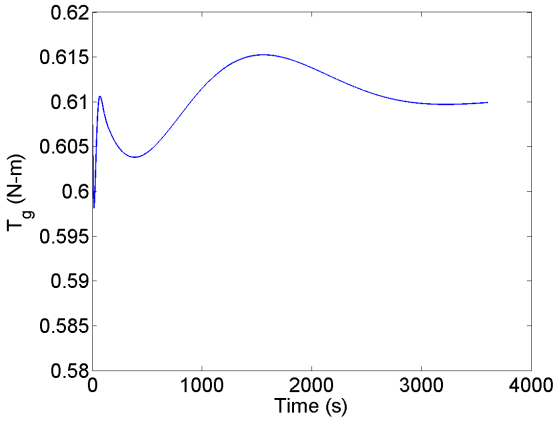

(c) Gimbal torque

Figure 7. System response of LQR controller with observer implemented, commanded $\alpha = 35°$

The LQR controller settles considerably better than the one with manually-placed poles using a SISO technique. The gimbal angle fluctuates more, but again settles to its trim state for the commanded α. The control effort is only slightly less than the first controller, but the LQR control effort fluctuates more (note the differing time scales on the torque plots).

The response of the LQR controller implemented with observer error can be seen in Figure 8.

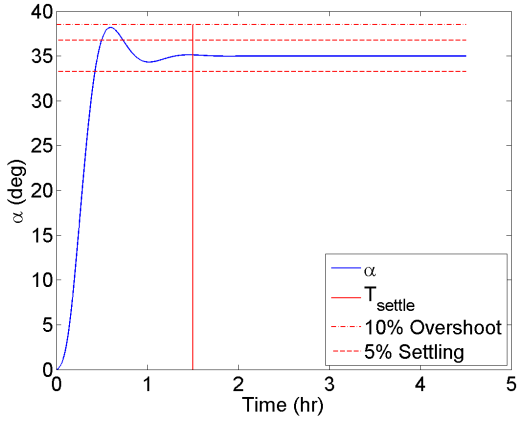

(a) α response

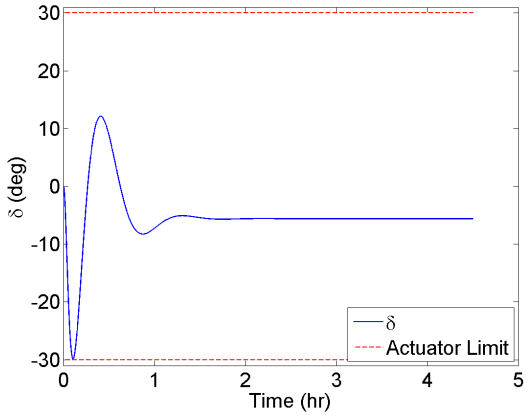

(b) δ response

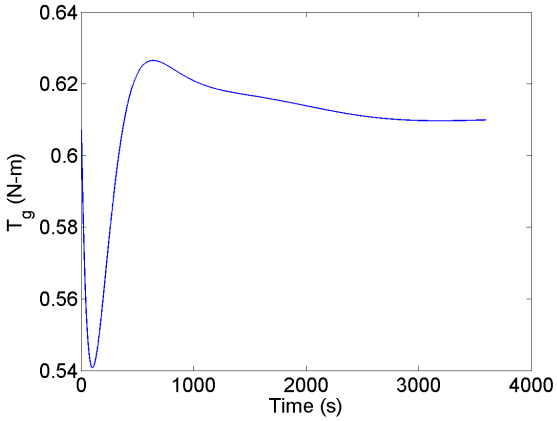

(c) Gimbal torque

Figure 8. System response of LQR controller with observer implemented, commanded $\alpha = 35°$, initial observer error

Despite observer error, the LQR controller still settles quickly. Gimbal angle comes very close to the limit, but is still within the boundary. The control torque is considerably less than the first controller's with the same observer error. The lesser control effort makes this response more desirable than the first controller's response. Observer error can be seen in Figure 9.

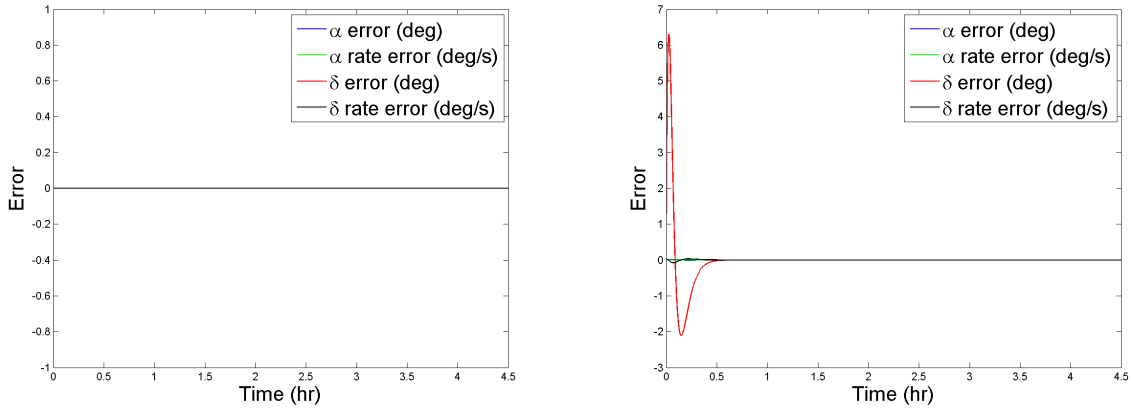

(a) No initial error

(b) 0.05° initial error in sun angle

Figure 9. Observer errors.

The observer error goes to zero in the same way the first controller-observer implementation did. Due to the difference being imperceivable, the difference in error is provided in Figure 10.

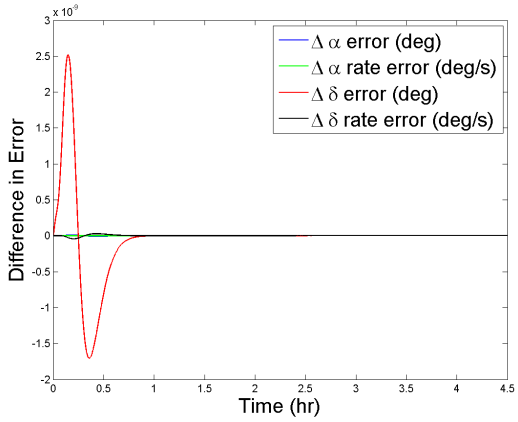

Figure 10. Observer errors with LQR control.

VI. Monte Carlo on Plant Errors

The most significant source of error between the real plant and the model is the offset between the sail center of mass and center of pressure [Wie]. Design constraints, unaccounted occultation, and sail billowing could all cause this offset, which introduces disturbance torques. For this analysis, an offset of up to 1 m of the center of pressure to the center of mass along the sail transverse axis is considered. Uniformly random variations were tested for 100 cases. Figure 11 shows the first controller in these cases.

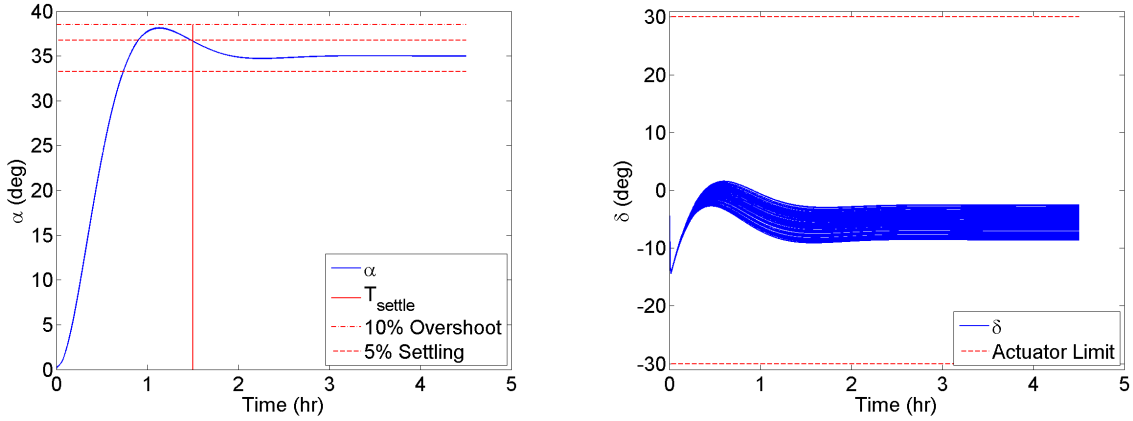

(a) α response

(b) δ response

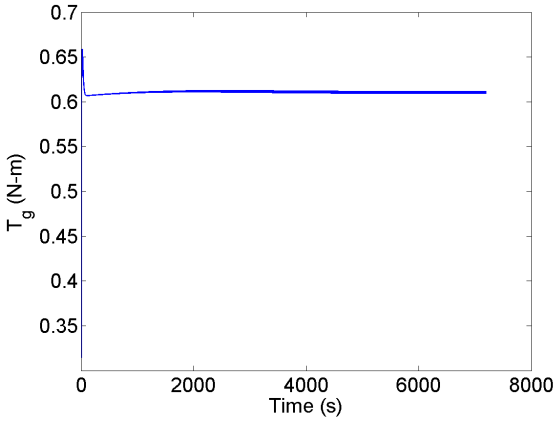

(c) Gimbal torque

Figure 11. System response of the first controller with observer implemented with random CM/CP offsets in plant, commanded $\alpha = 35°$

The controller was able to meet the design criteria even with the disturbance torque. Because the steady-state error is tracked and forced to zero, the sun angle meets its commanded state. The control torque shows a change in effort compared to without the disturbance. Figure 12 shows the LQR controller's response.

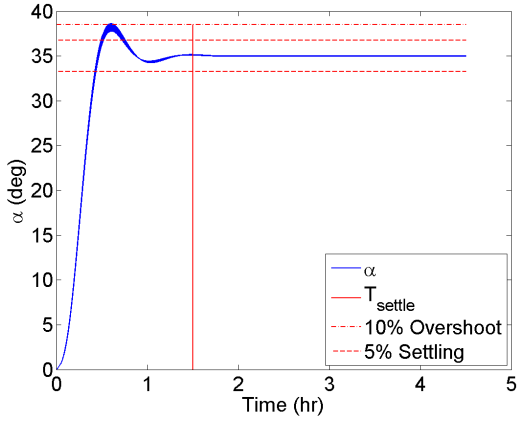

(a) α response

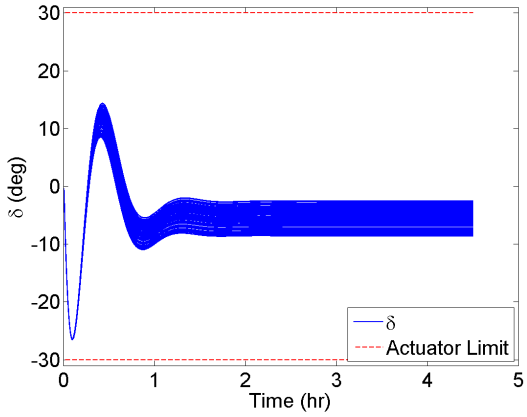

(b) δ response

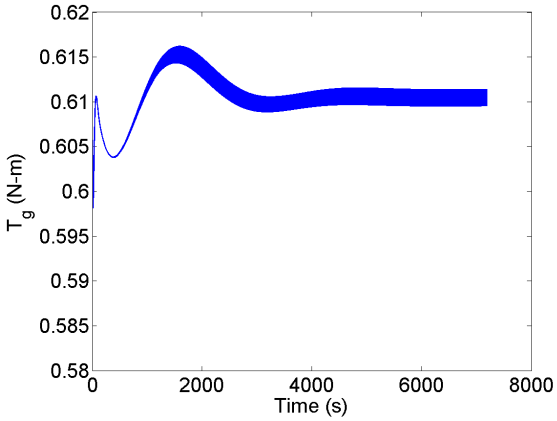

(c) Gimbal torque

Figure 12. System response of LQR controller with observer implemented with random CM/CP offsets in plant, commanded $\alpha = 35°$

The LQR controller was also able to meet the design criteria with disturbance torques. Steady-state error is forced to zero due to the integral term, and gimbal angle is quite similar compared to the undisturbed case. The gimbal torque shows the same range of effort as the first controller.

VII. Conclusion

The non-optimal controller was able to meet the design criteria without observer errors. However, it proved to not be as robust to such errors as the LQR controller. This is due to the control effort used in both controllers. The LQR design assigned a cost to control effort, so less was used. On the other hand, the non-optimal controller, which was tuned with SISO methods, was otherwise sufficient in meeting control objectives. Perhaps with sensor filtering, observer error could be reduced such that the control effort would also be reduced.

The Luenberger observer was able to reconstruct the entire state from only knowing the sun angle. The poles also drove initial (realistic) initial observer error to zero without forcing the actuator to violate its constraints.

The control methods presented were able to meet the design criteria for single-axis control of the specified solar-sail spacecraft. Further research should be done for both 2-axis gimballing and combining a gimbal

with sail vanes at the edges of the sail, as well as craft with more massive busses and perhaps a gimballed payload on the other side of the sail. With such research, design flexibility will allow viable missions with reduced time or resource cost.